3-D surface profile measurements of large x-ray synchrotron radiation mirrors using stitching interferometry

Lahsen Assoufid*[1], Michael Bray[2], Jun Qian[1], Deming Shu[1]
[1]Advanced Photon Source, Argonne National Laboratory, 9700 South Cass Avenue
Argonne, Illinois 60439, USA
[2]MB-Optique SARL, 26-ter, rue Nicolai, 75012 Paris, France

*Contact information: assoufid@aps.anl.gov; phone: (630) 252-2774, fax: (630) 252-9303

ABSTRACT

Stitching interferometry, using small-aperture, high-resolution, phase-measuring interferometery, has been proposed for quite some time now as a metrology technique to obtain 3-dimensional profiles of surfaces of oversized optical components and substrates.

The aim of this work is to apply this method to the specific case of long grazing-incidence x-ray mirrors, such as those used in beamlines at synchrotron radiation facilities around the world. Both fabrication and characterization of these mirrors would greatly benefit from this technique because it offers the potential for providing measurements with accuracy and resolution better than those obtained using existing noncontact laser profilers, such as the long trace profiler (LTP). Measurement data can be used as feedback for computer-controlled fabrication processes to correct for possible topography errors. The data can also be used for simulating and predicting mirror performance under realistic conditions.

A semiautomated stitching system was built and tested at the X-ray Optics Metrology Laboratory of the Advanced Photon Source at Argonne National Laboratory. The initial objective was to achieve a measurement sensitivity on the order of 1 μrad rms. Preliminary tests on a1m-long x-ray mirror showed system repeatability of less than 0.6 μrad rms. This value is comparable to that of a conventional LTP. The measurement accuracy was mostly affected by environmental perturbations and system calibration effects. With a fully automated and improved system (to be built in the near future), we expect to achieve measurement sensitivity on the order of 0.01μrad rms or better.

In this paper, after a brief review of basic principles and general technical difficulties and challenges of the stitching technique, a detailed description of the measurement setup is given and preliminary results obtained with it are analyzed and discussed.

Keywords: *Stitching interferometry, phase measuring interferometry, long trace profiler, optical metrology, x-ray mirrors, synchrotron radiation.*

1. INTRODUCTION

X-ray synchrotron radiation beamline mirrors are used for a variety of functions, such as power filtering, steering, focusing, or harmonic rejection. They are made of highly polished substrates that are typically 1 m long and a few centimeters wide, and they come in a variety of shapes and materials. Common shapes are flats and sagittal cylinders; typical materials are silicon, fused silica, zerodur, ULE glass, or other materials that can be polished to a high degree of figure and finish. The reflective surface is usually coated with one or several stripes made of several 100-Å-thick films of heavy elements such as Au, Pt, Pd, and Rh, which reflect hard x-rays when set at a few mrad incidence angles with respect to the incident beam.

Modern x-ray synchrotron radiation beamlines require mirrors with surface finish (i.e., surface roughness) and slope error better than 3 Å and 3 μrad, respectively. In many synchrotron radiation facilities around the world, the long trace profiler (LTP) is the instrument of choice for directly measuring the surface slope error of x-ray mirrors.[1] Most of mirror manufactures, however, use commercial phase-measuring interferometers (PMI), where the mirror mounted at a grazing-incidence angle and the surface slope error value is derived from the height measurement data. However, both techniques have some disadvantages: While the LTP is capable of measuring any aspheric surface with sensitivity on the order of 0.5 μrad, it can only provide a 1-dimensional (1-D) surface slope profile and has a

limited surface sampling distance (1 mm). Standard commercial PMIs, on the other hand, can provide 3-dimensional (3-D) surface measurements with nanometer accuracy and a few hundred micron lateral resolution, but their field of view is generally much smaller (typically 100 to 150 mm) than the size of a typical x-ray mirror (1 m). Therefore, the mirror has to be measured at a glancing incidence angle, which results in the following: a) the glancing angle spreads the sampling of surface measurement points by a factor $1/\sin\theta$ (θ being the glancing angle relative the surface) and decreases height sensitivity by the same factor; b) a return flat mirror is required to reflect the test beam back onto the interferometer detector, thus adding further complication to the measurements; and c) the overall measurement setup results in a longer beam path, which makes the system prone to thermal drift- and vibration-induced errors.

An alternative to the above methods consists of using a large PMI system with an aperture the size of the optic to be measured. Large PMI systems with a test beam diameter up to 800 mm have been built and can be commercially procured. However, they are expensive and cumbersome. Furthermore, because a large-aperture PMI is usually made by simply expanding the beam from a smaller-aperture PMI, the result is measurements with poor lateral resolution, and the system becomes less attractive as a tool for measuring long grazing-incidence x-ray mirrors, because only a few pixels are utilized in the lateral dimension of the mirror surface. Finally, such a large system would need a long stabilization time and a very good optical system to obtain the desired resolution.

A promising approach to achieving high-resolution measurements with nanometer accuracy required for next-generation x-ray mirrors is the technique that combines high-resolution interferometric measurements and stitching.[2-12]

The technique holds the potential for providing high-resolution surface topography with accuracy and resolution better than that of other existing noncontact profiling techniques. The obtained data can be valuable for mirror quality checks both during and after fabrication. For example, the data can be used to compute the deviation from a specified surface profile, and the result can be used as feedback for a computer-controlled polishing system. The surface data can also be used as input for simulating and predicting the performance of an optic under realistic conditions.

In this paper, we report experimental results obtained using a semiautomated stitching system built at the Advanced Photon Source (APS) x-ray optics metrology laboratory.

2. BASIC PRINCIPLE

The stitching concept is not new and has been the subject of many papers.[2-12] However, it has not been widely considered until recently, and the stitching option is now becoming available in many commercial metrology tools, such as roughness measuring instruments and scanning probe microscopes. Here we focus on its application to the specific case of long-grazing-incidence x-ray mirrors, such as those used in synchrotron radiation beamlines.

The basic principle of the stitching technique is quite simple: It consists of using a standard small-field-of-view, high-resolution interferometer to measure the surface of an oversized optic at a number of locations, resulting in overlapped subaperture measurements that cover the entire optical surface (Fig. 1). Then these subaperture measurements are stitched together with a computer program to construct a full 3-D surface profile.

Discussion on stitching algorithms can be found in references 9 and 10. The computer code used to stitch the data obtained in this work was developed by one of the authors.[12] The details of the algorithm will not be discussed in this paper. However, a brief description of the basic concept is as follows: The mathematical treatment consists of computing and subtracting individual tip-tilt piston functions ($f(x,y)ax+bx+c$, with a, b, and c being the stitching coefficients) from each subaperture measurement, and as a criterion for stitching quality, the software, in its present first version, uses the global rms of all height errors (along the vertical "z axis") over all pairs of overlapping subapertures.

One should be aware that the main (and almost the only) advantage of this criterion is its simplicity. Deriving second-order functions generates first-order functions, which are readily solved using matrix formulation. However, this linear processing implies that measurement errors are of Gaussian statistics. But if this were so, doors would never slam during measurement and air disturbance would be negligible. This is because such phenomena generate errors of amplitude many times the desired standard deviation (which is, say, 1 nm rms). According to Gaussian statistics, these “events” should hardly ever happen.

Next versions of the software will address this, using nonlinear processing. However, such processing can only be defined once the statistics of the measurement process are well known. This will require a number of trials.

A list of effects to be modeled includes:

- Small time-scale effects (vibration, air movement, etc.)
- Medium time-scale effects (atmospheric stratification during measurement, slow temperature changes, etc.)
- Large time-scale effects (imperceptible, negligible effect on measurement if taken into account)

As more measurements are performed, these effects will be modeled and included in our stitching software.

3. SOURCES OF ERRORS

3.1 General discussion and classification

There are numerous possible sources of errors, and a detailed discussion on these can be found in references 5 and 11. They can be classified as two types:[11] The first type contains those errors that are typical to interferometry, while the second type is more specific to the stitching process. Generally, the stitching process does not generate errors; the only potential problem is large-scale fluctuation resulting from the propagation of small errors from individual subaperture measurements, which in turn leads to imperfections in the overlap between individual measurements.[12] These errors are caused by: 1) the interferometer noise and nonlinear effects, 2) static errors resulting from a lack of calibration, and 3) dynamic errors, which include thermal and mechanical errors, etc.

The interferometer noise has been estimated to have a negligible effect (less than 0.001 μrad rms).[12] Nonlinear effects are, on the other hand, dependent on the design of the interferometer, and they are the most difficult to overcome. Static and dynamic errors are not insurmountable and can be easily minimized by proper design and calibration of the measurement system.

Figure 2 illustrates the effect of random errors. Figure 3 shows a 1-D stitching profile extracted from 3-D data measured with no proper thermal shielding of the measurement setup. A comparison with LTP measurement of the same mirror reveals a large discrepancy between the two profiles. The propagation of subaperture errors, which are due to improper thermal control and a lack of calibration, resulted in exaggerated mirror curvature.

3.2 Calibration effect

Obviously, calibration is required in order to perform interferometry. However, in the case of stitching, local calibration errors can propagate, thus generating large (albeit large-scale) errors. These will result in a global curvature, with local periodic errors.

A calibration curvature error stitches with no overlap error. Therefore, it only introduces an overall curvature which, once estimated, can be removed without any consequences to the mid- and small-scale features of the measured components.

Note, as mentioned above, it is not the stitching itself that generates such errors. However, stitching reveals the lack of calibration, as well as environmental phenomena.

If stitching reveals errors, it can also help to eliminate them. In short, we use the stitching hardware and software to acquire measurements with lateral displacement and perform some kind of "shearing interferometry." However, contrary to real shearing, noise is introduced in this process, and this must be taken into account by additional processing.

Absolute calibration, as we call the above method, was the subject of a previous paper.[11] New results will be reported when they are ready.

4. APPLICATION TO LONG GRAZING-INCIDENCE X-RAY MIRRORS

Stitching interferometry for “standard” large components usually means generating a 2-dimensional array of measuring locations. This prevents measurement errors from propagating, as each subaperture is constrained somewhat by its numerous surrounding neighbors (Fig. 1).

This is not the case for long gazing-incidence x-ray mirrors, for which the subaperture topography is reduced to 1-D, and a single error will propagate fully. (In Fig. 4, the error in "A" propagates to the edges of the component.)

The solution for this is to perform "double-overlap,"[12] whereby each overlap is completely constrained by an independent subaperture (In Fig. 5, the error in "A" is reduced by the large overlap.) This also provides better lateral coverage of wide optics, allowing, e.g., 90-mm-wide mirrors to be adequately measured with a 100 mm interferometer.

5. MIXED STITCHING

Even with proper system calibration, thermal fluctuations can degrade the overall figure ("large-scale" errors) by a slight, but sometimes unacceptable, amount.

It could also be possible that overall figure could be known by some other means:

- Long trace trofiler;
- Glancing angle interferometry (large-scale, low-resolution);
- etc.

The stitching software used in this work has the ability to mix, in a single stitching sequence, data from various sources and formats. This can lead to faster and more accurate measurement sequences, because the propagation of local errors will be neutralized by the overall large-scale measurement, which, in turn, can be performed in a single take (e.g., using glancing measurements). Thus, the subaperture measurements can be performed without stringent environmental conditions.[12]

6. MEASUREMENT SETUP

For this initial test, we chose to use standard components that were readily available to the metrology laboratory. A photograph of the measurement setup is shown in Fig. 6. It consists of a standard PMI-WYKO-6000 Fizeau interferometer, a long translation stage, a fringe-adjustment assembly (made of a tip-tilt and rotation platforms), and a mirror-mounting platform.

The interferometer has a 150-mm-diameter aperture. We chose to keep the interferometer fixed and scan the mirror. The drawback of this option is that the translation stage travel has to be at least twice the mirror length. However, x-ray mirrors are generally much lighter than the interferometer, and so they are much easier to translate than the interferometer. The translation stage has a resolution of 2 μm and a repeatability of 10 μm with a maximum travel of 800 mm. The interferometer detector has 256 x 256 pixels with a pixel size on the order of 0.586 mm at the test beam aperture. The stage has, therefore, sufficient accuracy and repeatability to position the mirror within less than 1/10 of a pixel, thus avoiding possible positional stitching errors.

In order to reduce environmental perturbations (temperature drift and air turbulence), the complete setup, including the mirror and the translation stage, was housed in a Plexiglas enclosure. A window, the size of the interferometer test beam, is provided at the center of one of the Plexiglas sidewalls to let the laser beam into the enclosure at normal incidence to the test mirror surface. The interferometer exit lens and the enclosure sidewall were linked together by a soft shroud to minimize propagation of vibration and deformation. To avoid parasitic laser reflection, the enclosure inner walls were covered by black mat paper.

The translation stage was actuated by a stepping motor through a VME crate and the interferometer's computer. Because the fringe adjustment assembly (the tip-tilt and rotation platforms) was not motorized, a door (flap) was provided at the top of the enclosure to access the tip-tilt and rotation platforms in order to null the fringes prior to interferogram acquisition at each measurement location.

7. MEASUREMENT AND RESULTS

7.1 Measurements

The measurements reported here were performed on a 1-m-long, 40-mm-wide, and 40-mm-thick silicon x-ray mirror. Its surface was polished down to 2 Å rms, and the residual slope error was specified to 1 μrad rms. The mirror was first measured using the LTP, and the residual surface slope was found to be on the order of 2 μrad rms.

Because of stage travel limitations, the stitching measurements were performed only over a 600 mm length. Several sets of measurements (in a single overlap mode) were acquired in the following manner:

- A set of two consecutive measurements with no averaging at each measurement stop. (i.e., a single interferogram was acquired at each subaperture location).
- A set of two consecutive measurements where 10 interferograms were taken and averaged at each subaperture location.

Because the diameter of the test beam was much wider (150 mm) than the width of the mirror, the mirror was only scanned along the tangential direction (1-D stitching case).

The size of the overlap area (between adjacent subapertures), as well as the number of measurements, can greatly influence the accuracy of the measurement.[5] A very large overlap area means a large number of measurements and a rapid increase in measurement time. As a result, the measurements become prone to errors. A very small overlap area leads to a short measurement time, but it is likely to increase imperfections in the stitched data.

7.2 Results and discussion

After all of the subaperture measurements were completed, the data were processed using the stitching algorithm.

Tables 1 and 2 summarize the results. Table 1 gives the surface statistical parameters without curvature removal. Table 2 shows the result after the average curvature is computed and subtracted from the stitched surface profiles.

"VALUE differences" are the differences obtained by subtracting statistical values of two different measurement data sets, and "MEASUREMENT differences" are the values obtained after subtracting two different measured data sets and then computing statistical values of the resulting difference data set.

The mirror showed a slope error of about 3 μrad rms before the average curvature was subtracted, and less than 1.6 μrad rms after the best-fit radius of curvature was subtracted from the original stitched profiles. For comparison, LTP measurements taken along the mirror axis gave a residual slope error of 2 μrad rms.

The average radius of curvature varies from 55.47 to 56.13 km, depending on the scan (see Table 2). The rms values of the profiles obtained by subtracting any two different stitched profiles are less than 0.6 μrad rms. This value is comparable to that of the LTP. The rms values obtained from the difference between rms values of any two different measurement profiles varies from 0.01 to 0.08 μrad, which is mostly attributed to environmental effects.

Finally, the slope error derived from the stitched data ("MEASUREMENT difference") shows an improvement of a factor of 2 between nonaveraged and 10averaged measurements.

- (av1-b) – (av1-a) = 0.59 μrad rms;
- (av10-b) – (av10a) = 0.30 μrad rms.

This factor of 2, reasonably close to $10^{\frac{1}{2}}$ (considering the complexity of the whole operation), points to random effects as the cause of the slope error. If this were correct, thermal phenomena would be the cause of such error, which would be consistent with previous observations.

Another observation is the extremely low value of "VALUE differences" compared to "MEASUREMENT differences." This points to a random phenomenon with constant statistical characteristics. No more can be implied at this time.

Figure 7 shows an example of the surface slope profile computed from the stitched data. Note that the residual surface profile reveals imperfections affecting the stitching process. These imperfections are attributed to thermal drift and (as manifested by periodic patterns) calibration (i.e., static) errors.

Finally, note also the usefulness of the 3-D surface slope in revealing scratches and other fabrication and polishing defects.

8. CONCLUSIONS

A semiautomated stitching interferometry system has been built and successfully tested on a long x-ray synchrotron radiation mirror. The aim of this work was to achieve slope measurement sensitivity on the order of 1 μrad rms. The preliminary tests have demonstrated a system repeatability that is less than 0.6 μrad rms, a value that is comparable

to that of the LTP. Value differences are even lower, never exceeding 0.05 μrad rms, when power is removed. The obtained results were particularly encouraging because the measurements were performed with a nonoptimized setup.
With a fully automated system (to be built in the near future) and further enhancement to the stitching code, combined with proper system calibration, we expect to achieve slope measurement sensitivity on the order 0.01 μrad rms or better.

ACKNOWLEDGMENTS

One of the authors, Lahsen Assoufid, would like to thank Kurt Goetze for technical assistance. This work is supported by the U.S. Department of Energy, Office of Science, Basic Energy Sciences, under contract No. W-31-109-Eng-38.

REFERENCES

1. P.Z. Takacs, S.N. Qian, J. Colbert, Proc. SPIE **749** 59 (1987).
2. J.E. Negro, "Subaperture optical system testing," Appl. Opt. **23**(12) 1921-1930 (1984).
3. M. Bray, "Stitching Interferometry for large plano optics using a standard interferometer," Proc. SPIE **3134** 259-273 (1997).
4. Y.J. Fan, K.G. Struik, P.C. Mulders, C.H.F. Velzel, "Stitching Interferometry for the Measurement of Apsheric Surfaces," *Annals of the CIRP* **46**/1 459-462 (1997).
5. J.C. Wyant and J. Schmit, "Large Field of View, High Spatial Resolution, Surface Measurements," *International Journal of Machine Tools Manufacturers*, Vol. **38** 691 (1998).
6. M. Bray, Stitching interferometer for large optics: Recent developments of a system," Proc. SPIE **3492**, 946-956 (1998).
7. A. Fanning, "Polished Homogeneity of Corning Fused Silica Boules," Proc. SPIE **3872**, 453-463 (1999).
8. M. Bray, "Stitching Interferometry: how and why it works," Proc. SPIE **3739** 259-273 (1999).
9. M. Otsubo, K. Okada, J. Tsujiuchi, "Measurement of large plane surface shapes by connecting small-aperture interferograms," Opt. Eng. **33**(2), 608-613 (1994).
10. M. Sjodahl, B.F. Oreb, Opt. Eng. **41**(2), 403-408 (2002).
11. M. Bray, "Stitching Interferometry and Absolute Surface Shape Metrology: Similarities," Optical *Manufacturing and Testing IV*, Proc. SPIE **4451,** 375-383 (2001).
12. M. Bray, "Stitching Interferometry for the Wavefront Metrology of X-ray Mirrors Proc. SPIE **4501,** 63-67 (2001).

Table 1. The stitched measurements with no curvature subtracted from the data. av1-a & av1-b are measurements with no averaging, and av10-a and av10-b are measurements obtained by averaging 10 interferograms at each subaperture location. "VALUE differences" are the differences obtained by subtracting statistical values of two different measurement data sets, and "MEASUREMENT differences" are the values obtained after subtracting two different measured data sets and then computing statistical values of the resulting difference data set.

		Height (nm)		Slope (μrad)	
		P-V	rms	P-V	rms
Individual measurement sets:	av1-a	1148	**290**	40.9	2.93
	av1-b	1152	**291**	38.3	2.94
	av10-a	1192	**306**	37.0	3.06
	av10-b	1183	**302**	38.3	3.02
VALUE differences:	(av1-b) - (av1-a)	4	**1**	-2.6	**0.01**
	(av10-b) - (av10-a)	-9	**-4**	1.3	**-0.04**
	(av1-a) - (av10-a)	-44	**-16**	3.9	**-0.13**
	(av1-b) - (av10-b)	-31	**-11**	0.0	**-0.08**
MEASUREMENT differences:	(av1-b) - (av1-a)	66.5	**5.1**	42.30	**0.59**
	(av10-b) - (av10-a)	45.8	**6.4**	28.10	**0.30**
	(av1-a) - (av10-a)	97.1	**17.4**	50.00	**0.60**
	(av1-b) - (av10-b)	82.3	**12.2**	46.70	**0.59**

Table 2. The stitched measurement after the best-fit radius is subtracted from the data. av1-a & av1-b are measurements with no averaging, and av10-a and av10-b are measurements obtained by averaging 10 interferograms at each subaperture locaton. "VALUE differences" are the differences obtained by subtracting statistical values of two different measurement data sets, and "MEASUREMENT differences" are the values obtained after subtracting two different measured data sets and then computing statistical values of the resulting difference data set.

		Best Fit Radius (km)	Height (nm)		Slopes (μrad)	
			P-V	**rms**	P-V	**rms**
Individual measurement sets:	av1-a	56.133	401.0	**63.7**	40.8	1.53
	av1-b	55.938	423.0	**67.3**	36.4	1.58
	av10-a	54.061	407.0	**64.0**	35.9	1.51
	av10-b	54.472	421.0	**66.2**	38.1	1.54
VALUE differences:	(av1-b) - (av1-a)		22.0	**3.6**	-4.4	**0.05**
	(av10-b) - (av10-a)		14.0	**2.2**	2.2	**0.03**
	(av1-a) - (av10-a)		-6.0	**-0.3**	4.9	**0.02**
	(av1-b) - (av10-b)		2.0	**1.1**	-1.7	**0.04**
MEASUREMENT differences:	(av1-b) - (av1-a)		67.4	**4.9**	42.3	**0.59**
	(av10-b) - (av10-a)		33.8	**3.9**	28.1	**0.30**
	(av1-a) - (av10-a)		64.9	**4.3**	50.0	**0.59**
	(av1-b) - (av10-b)		58.1	**2.5**	46.7	**0.58**

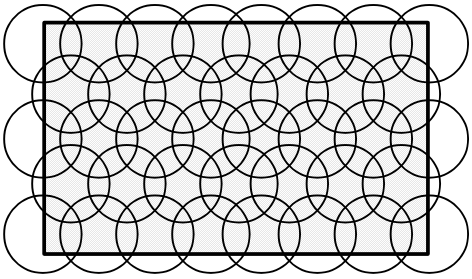

Fig. 1. Principle of the stitching technique.

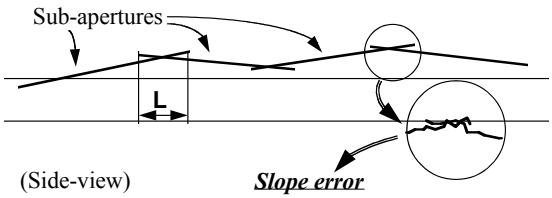

Fig. 2. Illustration of the random noise effect.

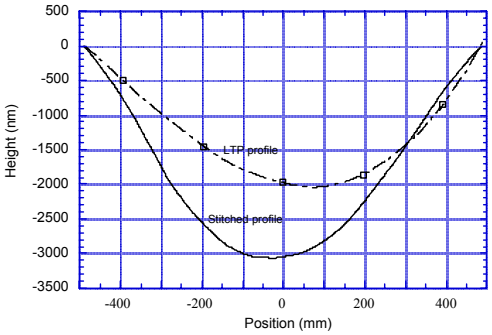

Fig.3. Effect of local thermal perturbations on the stitched global profile: the stitched profile showed an exaggerated curvature compared with the LTP measured profile on the same mirror.

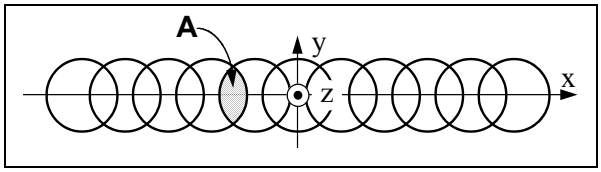

Fig. 4. Single overlap (error generating).

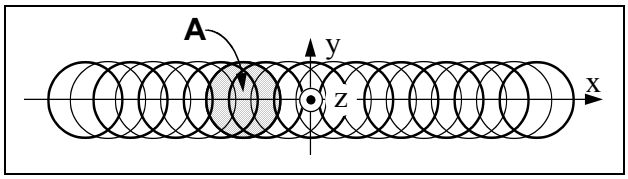

Fig. 5**.** Double overlap (much less error generating).

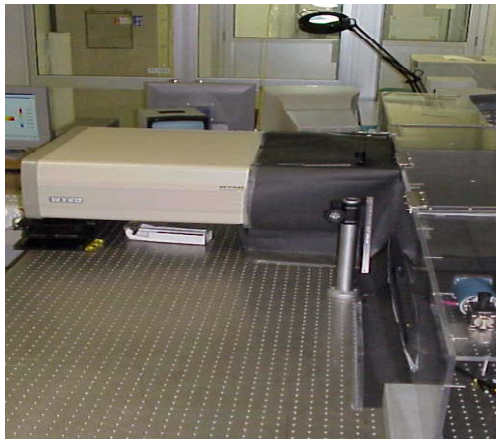

Fig. 6. Photograph of the stitching setup.

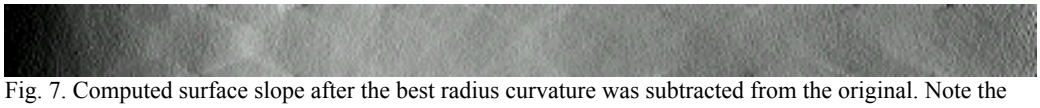

Fig. 7. Computed surface slope after the best radius curvature was subtracted from the original. Note the imperfections, due to the system and calibration errors, revealed by the stitching process. Note also the usefulness of a 3-D slope profile in revealing possible scratches and other polishing defects.